Analysis of Propagation for Wireless Sensor Networks in Outdoors

Giselle M. Galvan-Tejada[1, 2, *] and Jorge Aguilar-Torrentera[3]

Abstract—A revision of main propagation mechanisms of radio waves for wireless sensor networks is presented in this paper. In order to address this topic, the free space model is firstly taken as a reference. Classical concepts like ground reflection, diffraction, and surface waves are included from a theoretical point of view, and some aspects related to wireless sensor networks are analyzed for each subject. A key parameter is the height of antennas which plays an important role on distinct formulations like reflection coefficient of the ground surface. From there, when antennas are very close to ground surface, the far field conditions could be different from that typical expression. Hence, some of propagation models involve a characterization of far field conditions, and practical settings of antennas for wireless sensor networks are analyzed by electromagnetic simulation. Attenuation due to vegetation is also reviewed, and models suitable for these networks are exposed.

1. INTRODUCTION

Nowadays Wireless Sensor Networks (WSNs) have become a mature technology, which is being developed in diverse scenarios from aerospace, terrestrial to underground environments [1–7], for applications as precision agriculture, smart grids, security, surveillance, habitat monitoring, health sensing and educational activities. The grade of growth of WSNs has allowed the arising of Internet of Things (IoT), which will be incorporated to the next generation of cellular mobile communications also known as 5G [8, 9]. Moreover, new designs of antennas for WSN have been proposed [10], and some of them are based on ultra-wideband (UWB) technology for their use in a much wider span of frequencies, always taking into account the interference constraints (see [11] for instance).

On the other hand, propagation is always a central issue not only for the antennas and propagation community, but also for the whole wireless communications area. Then, due to the importance of WSNs, this paper analyzes subjects of radio wave propagation for these networks provided that some classical models cannot be used in them because they have been developed for different conditions.

Thus, the peculiarities of the radio wave propagation for WSNs from an electromagnetic point of view are analyzed, and comments are presented. In this concern, since WSNs can be found in almost any environment, a study including all possible cases would exceed the length of a regular paper like this. To solve this detail, a typical classification depending on their applications both indoors and outdoors can be done. From this division, we choose to concentrate this paper only on propagation characteristics for outdoor scenarios. Works related to wireless sensor networks usually assume simple propagation conditions, and some important features are not contemplated, like antennas heights. In this paper, the conjunction of different subjects of radio wave propagation into the topic of wireless sensor networks is presented pointing out key characteristics that should be taken into consideration.

The paper is then organized as follows. Section 2 describes some physical particularities of scenarios for WSNs. A central parameter that determines many aspects in the radio wave propagation is the

operational frequency, hence the corresponding references of the standard where different frequency bands are defined are also included in this section. A general explanation of propagation mechanisms found in outdoors environments is addressed in Section 3. Free space propagation condition and its model are explained in Section 4. Due to some typical applications of WSNs where nodes are relatively near of ground, it is important to review the far field characteristics under this condition. Thus, Section 5 addresses this subject. Section 6 presents the two-ray model derived from the effect of ground reflection over a plain Earth. Based on the above, the physical and mathematical explanations for the two-slope model are exposed in Section 7 including some comments on its use in WSNs. The diffraction phenomenon for wireless sensor networks is revised in Section 8, where some details of the recent approach taken in [12] are highlighted. The relative closeness of nodes to the ground also motivates us to address some particularities of the surface waves as explained in Section 9, where definitions provided in the investigation on the topic and approaches proving the absence of surface waves are included. Aspects associated with vegetation and some path loss models adopted for WSNs are reviewed in Section 10. From these, the work published in [13] is outstanding for the analysis done for the standard used in WSNs. In addition, considerations for the design of these networks in a complex environment, where a combination of tree species, age, spatial distribution, and closeness to buildings as addressed in [14], are also commented in this section. Concluding remarks are given in Section 11.

2. ENVIRONMENTS OF DEPLOYMENT FOR WIRELESS SENSOR NETWORKS

The development of small size low-cost devices for WSNs has allowed that these networks can be deployed in almost any environment. The common characteristic is that each device is power limited (maximum transmission level in the order of 100 mW [15]), in such a way that their range is relatively short. Naturally the strength of WSNs is its cooperative operation, which makes them able to cover wide areas by implementing dozens or hundreds of sensors. Depending on the situation, their nodes can be distributed on a random basis (for disaster cases) or following a specific planning (home monitoring, industrial monitoring, etc.).

2.1. IEEE802.15.4-2011 Standard

IEEE802.15.4-2011 [16] is a standard for low-power and low-rate technology used by wireless personal networks, from which WSNs are a very illustrative example. This standard defines the physical layer (PHY) and medium access control layer (MAC). In its PHY different frequency bands are defined at the most popular 868 MHz, 915 MHz and 2.4 GHz, although an expansion of more bands can be found in its revised version published in 2016 [17]. In this concern, this paper will be focused on the 2.4 GHz band provided the existing commercial development in the market.

2.2. Characteristics for Outdoor Scenarios

Wireless sensor networks in outdoor scenarios have a wide diversity of applications such as intelligent transportation systems, agriculture, environmental monitoring, among others. The propagation paths between nodes will find natural and man made obstructions. Atmospheric conditions could play a certain role. Heights of nodes can be under, at, and above ground level, and their separations can be relatively short, from a few meters up to one hundred meters depending on the power capability of each device.

3. FUNDAMENTALS OF PROPAGATION MECHANISMS IN OUTDOOR SCENARIOS

In principle, the propagation of radio waves in outdoor scenarios can be given via different paths, and depending on them, the waves will be known by different names [18]: (i) when a signal travels via a reflection mechanism on the ionosphere layer of atmosphere, it is called *sky wave*; (ii) when scattering is present in the troposphere around 10 km above the Earth's surface, *tropospheric waves* can be found; (iii) when the waves propagate through other paths on the troposphere relatively near the Earth's

surface, they are known as *ground waves*. The propagation mechanisms of ground waves include direct paths, reflection on ground or other objects, diffraction, and a special condition known as *atmospheric ducting* caused by changes on the refractive index depending on the temperature, humidity, and pressure conditions [19]. Ionospheric propagation, tropospheric waves, and atmospheric ducting are not issues considered for WSNs, so, we shall be concentrated on the other propagation mechanisms for ground waves, which together are named *space waves*.

Before addressing details of propagation mechanisms of space waves, it is worth presenting some generalities involved between the transmitted signal and its counterpart received: mean received power (related to the average path loss), large-scale fading or shadowing, and small-scale fading, whose relationship is graphically depicted in the simulated plots of Fig. 1, where the received power of a signal as a function of separation between antennas is shown (the frequency of 100 MHz used to obtain the plots of free space and slow fading in this figure was taken only as an example to illustrate the different scales of these phenomena). For the sake of simplicity, unitary gain antennas were used in the simulations of this figure. It is worth noting that the model used to simulate the mean received power is valid for distances at which electromagnetic fields are described by plane waves propagating through the space, and the far field condition is met. This implies that the transmitter and receiver are placed at a distance at which the antennas are not coupled by effects associated with reactive energy stored in the near field of each antenna. This problem is analyzed in this paper in Section 5.
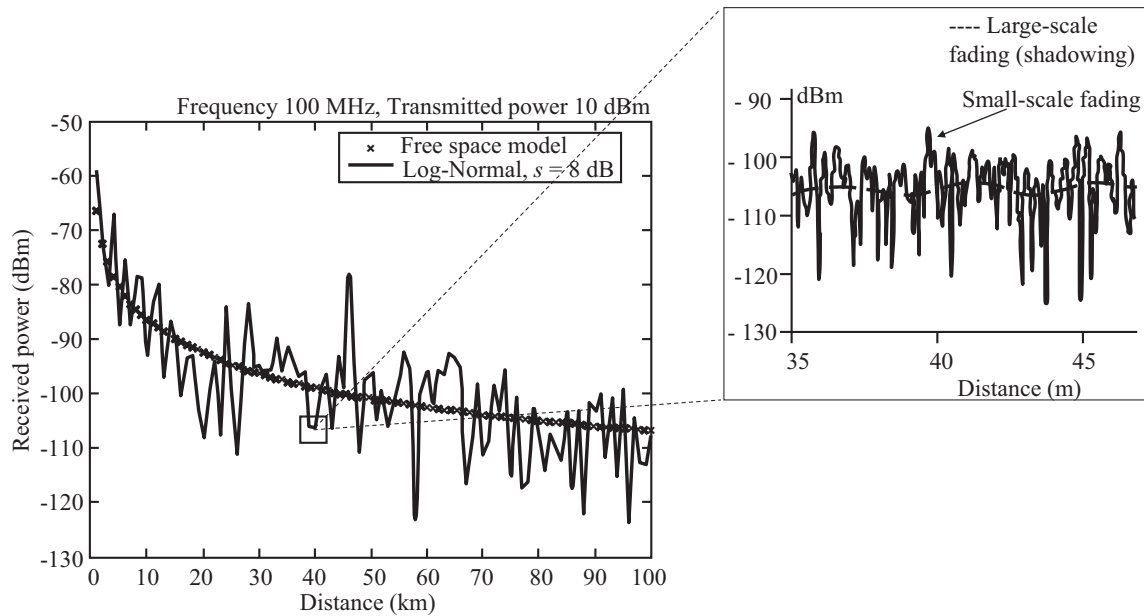

Figure 1. Mean received power, shadowing and small-scale fading.

Let us now explain the physical meaning of curves illustrated in Fig. 1. First of all, there is a certain power decay of the transmitted power as a function of the distance, which is determined by propagation models of *average* path loss depending on the analyzed scenario. In the case of Fig. 1, for example, we use a free space model, where, as explained in Section 4, antennas are located in an environment without any obstruction or atmospheric absorption in the propagation path (naturally there can exist other models for the average path loss, as can be found in a recent reference of this topic for WSNs [20]).

Around this mean received power, there exists a long-term variation of the level of the received power depending on if the signal experiments diffraction through the propagation path due to buildings, trees, mountains, etc. in such a way that an "electromagnetic shadow" can be presented around obstacles according to relative positions between transmitter and receiver. This phenomenon is statistically characterized and has been found to follow a Log-Normal distribution, whose standard deviation, s, provides a statistical measure of the grade of obstructions in the environment (in Fig. 1, a Log-Normal distributed random variable with $s = 8$ dB was simulated). The diffraction phenomenon represents the

deterministic form of the long-term fading. A brief description of this phenomenon can be found in Section 8 below.

Finally, the small-scale fading is a phenomenon caused by a set of possible echoes of the first signal arriving at the receiver, which could follow a direct line of sight (LOS) path. These multiple echoes are attributed to scattering objects that produce reflections or diffraction on the propagation paths of the original signal, and therefore they create a multipath environment. These replicas vary both in amplitude and delay, in such a way that they can be constructively or destructively added depending on their relative phases. Ndzi et al. [21] present some observations derived from a measurements campaign for WSN applications in sport ground, grass field, and roads for relatively short ranges and antennas near surface. A Ricean distribution is found to be best adjusted for the small-scale fading up to distances close to the transmitter with some variations depending on the surface characteristics. In Section 6, an explanation of reflection in the ground is exposed from the radio wave propagation point of view. Many of the concepts reviewed there can also be considered for reflection at buildings or other materials.

The scale of variation of signal due to both types of fading is worth noting (see Fig. 1): shadowing is present in a larger scale compared to small-scale fading, and therefore, they are sometimes referred as long-term and short-term fadings, respectively [22].

In addition to these three characteristics on the propagation paths, the atmospheric absorption can be present in distinct cases, but naturally its effect is observed for signals being transmitted outdoors only.

In any case, a common factor in all above propagation effects is operational frequency, which determines the impact of these phenomena on the received signal and other metrics of performance of a wireless system.

The orientation that we are giving to this paper is from a deterministic point of view of the mean received power, reflection, and diffraction. In other words, we are not addressing the shadowing effect as can be found in classical literature, nor the statistical modeling corresponding to small-scale fading due to multiple reflections. Instead, we present theoretical formulations including some remarks related to the particularities of WSNs.

4. FREE SPACE

Free space is a propagation condition where a signal emitted from an isotropic source will not find any obstruction, scattering or atmospheric absorption that introduce attenuation, in such a way that the wave freely spreads its energy equally in all directions (the corresponding model presented below is used in Fig. 1). This condition implies that the radio wave travels in a perfect dielectric without charges and conduction currents [18]. Under these circumstances, the wave equations for the electric field and magnetic field vectors, **E** and **H**, respectively, are [23]:

$$\nabla^2 \mathbf{E} - \mu\varepsilon\frac{\partial^2 \mathbf{E}}{\partial t^2} = 0 \tag{1}$$

$$\nabla^2 \mathbf{H} - \mu\varepsilon\frac{\partial^2 \mathbf{H}}{\partial t^2} = 0 \tag{2}$$

where ε denotes the dielectric constant, μ the magnetic permeability, and ∇ the vector differential operator. The possible solution of Eqs. (1) and (2) describes a plane wave in a direction of propagation perpendicular to the surface formed by vectors **E** and **H**, which are normal from each other. This solution and all equations derived from now on are valid for *far field conditions* to be presented in Section 5.

The magnitudes of the electric field, E, and the magnetic field, H, are related to each other by,

$$\frac{E}{H} = \sqrt{\frac{\mu}{\varepsilon}} \tag{3}$$

Due to the dimensions of magnitudes E (V/m) and H (A/m), Equation (3) represents an impedance quantity in Ohms. In particular, it is known as the *characteristic impedance* or *intrinsic impedance* of the medium, η. For free space, $\varepsilon_0 \approx 1/36\pi \times 10^9$ F/m and $\mu_0 = 4\pi \times 10^{-7}$ H/m [18], hence, its

characteristic impedance is

$$\eta_0 = \sqrt{\frac{\mu_0}{\varepsilon_0}} = 120\pi \approx 377\,\Omega \tag{4}$$

On the other hand, the well-known Poynting's theorem provides an insight of the energy conservation between energy supplied to the field and energies stored in the electric and magnetic fields plus the energy flow through the surface that encloses that field [24]. Thus, *"As electromagnetic waves propagate through space from their source to distant receiving points, there is a transfer of energy from the source to the receivers."* [18]. In other words, the Poynting's theorem mathematically represents the relationship between the rate of this energy transfer and amplitudes of electric and magnetic fields of the electromagnetic wave. This representation includes a closed surface integral of the product $\mathbf{E} \times \mathbf{H}$, which gives the rate of the energy flow through that enclosing surface [18]. Then, the Poynting vector, given by,

$$\mathbf{P} = \mathbf{E} \times \mathbf{H} \tag{5}$$

at any point provides a measure of the rate of the energy flow per unit area at that point. Let $\mathbf{E}_0$ and $\mathbf{H}_0$ be fixed amplitudes of $\mathbf{E}$ and $\mathbf{H}$, respectively, which is a valid assumption for plane waves propagating in free space. Let us also consider time variations of the form $\cos(2\pi f t - \alpha)$, with f the field frequency in Hz and α a phase parameter with fixed numerical value at any given point in the medium. This time variation of $\mathbf{P}$ can be simplified if an average is taken over time $1/f$, as long as $\mathbf{E}_0$ and $\mathbf{H}_0$ remain constant. Hence:

$$\mathbf{P}_{av} = \frac{1}{2}\mathbf{E}_0 \times \mathbf{H}_0 \tag{6}$$

Let P_{av}, E_0 and H_0 be the corresponding scalar magnitudes of vectors given in Eq. (6), such that,

$$P_{av} = \frac{1}{2}E_0 H_0 \tag{7}$$

Then, by using Eq. (3) into Eq. (7)

$$P_{av} = \frac{E_0^2}{2}\sqrt{\frac{\varepsilon}{\mu}} \tag{8}$$

Provided that we are assuming an isotropic source, the signal travels, spreading its energy equally in all spatial directions closed by an imaginary sphere. Thus, if the transmitter is supplying a power P_t at the terminals of an isotropic antenna, conceptually the power flux density (P_{av}) at a radial distance, d, can be expressed as,

$$P_{av} = \frac{P_t}{4\pi d^2} \tag{9}$$

Hence it is straightforward to find a relationship between the magnitude of electric field E_0 and transmitted power P_t by equaling Equations (8) and (9).

Through this section we have revised some expressions and concepts of radio waves under the free space condition, but using the term "reception point" as a general form to make a reference where the electromagnetic field is. In order to be more specific, it is necessary to first present the concept of *effective aperture* or *effective area* of an antenna. This concept is related to a receiver antenna provided that it represents the proportion between power flux density of a plane wave and the power effectively supplied to the antenna terminals. Mathematically it can be formulated as

$$A_e = \frac{P_r}{P_{av}} \tag{10}$$

where P_r denotes the received power (i.e., the power supplied to the antenna terminals). Then, it is clear that

$$P_r = A_e P_{av} \tag{11}$$

Some examples of effective areas for different radiators can be found in [25], from which for an isotropic antenna we have:

$$A_e = \frac{\lambda^2}{4\pi} \tag{12}$$

with λ being the wavelength. Thus, by substituting Eqs. (9) and (12) in Eq. (11), the expression of received power for free space conditions using isotropic antennas results:

$$P_r = P_t \left(\frac{\lambda}{4\pi d} \right)^2 \tag{13}$$

which is also known as *Friis Equation*. If we consider antennas with a certain gain, let us say G_t and G_r for the transmitter and receiver, respectively, these factors can be directly introduced into Eq. (13):

$$P_r = P_t G_t G_r \left(\frac{\lambda}{4\pi d} \right)^2 \tag{14}$$

with $G_t = 1$ and $G_r = 1$ for isotropic antennas. As can be observed, the power decay in this model is a function of distance and frequency only. For this reason it can be seen that the wave follows in a direct LOS path in the propagation environment. Please note that Equations (13) or (14) are valid only for far field, and no considerations are taken about heat losses and scattering losses of the antenna, for which we suggest [26] for a deeper discussion.

5. FAR FIELD CONDITIONS

5.1. Motivation

Provided that some applications of WSNs require that their nodes are relatively close to the ground, it is important to review the far field concept. The condition given for the far field is widely used as a rule of thumb. Nevertheless, some considerations should be taken into account as pointed out by [28]. In this concern, characterizations of a dipole antenna of various lengths and the transition boundaries between near field and far field have been systematically studied in [28] and also including a wire antenna array of half-wave dipoles in [29]. Based on numerical simulations (using the electromagnetic code *Analysis of Wire Antennas and Scatterers*, AWAS), these studies characterize the propagation of radiated energy from the near field to far field regions transition at larger distances than that stated in the standard [27].

5.2. Simulations

Here we characterize the far field of an antenna by considering a center-fed dipole operating at a frequency of 2.45 GHz (i.e., $\lambda = 12.24$ cm). We analyze the case of a dipole of length equal to 0.46λ. Ideally, in a free space circumstance, an infinitely thin 0.46λ dipole antenna resonates as its impedance has a zero reactive component at the operating frequency [30]. When the dimensions of such a dipole antenna change, the time-averaged radiated power has both real and imaginary parts increasing the spatial distribution of the reactive field stored near the dipole. Thus, by taking into consideration all above, we illustrate the transition between near field and far field of a 0.46λ-dipole antenna of diameter equal to 5 mm by carrying out full-wave EM simulations with the electromagnetic code COMSOL (RF module, COMSOL TM Version 5.2).

For free space conditions, the numeric technique yields an input impedance equal to $71.19 + j16.43$ Ohms. Since such a reactive component cannot be neglected, electrical and magnetic fields cannot have a spatial orientation settled down by the intrinsic impedance of the medium in close proximity to the antenna but at larger distances as one moves away from the antenna.

A property of the antenna operating at far field is that the wave impedance approximates to the intrinsic impedance of the media [29], which is numerically close to 120π as explained in Section 4. As noted there, $\eta = E/H$, so, the wave impedance of the field is equal to the ratio E_θ/H_ϕ, with E_θ the component of the magnitude of the electric field at an angular direction θ and H_ϕ the component of the magnitude of the magnetic field at the azimuth angle ϕ.

Figure 2 shows the variation of the real part of the field impedance with distance (normalized to the wavelength) for two angular directions θ (45° and 90°) under free space conditions. Theoretically, for such a dipole antenna radiating in free space, the far field starts from $2D^2/\lambda$, with D being equal to the dipole length 0.46λ. This ratio yields a distance equal to 0.423λ. Nonetheless, our results show that the far field condition is reached for both angular directions at a distance approaching λ. The conclusion
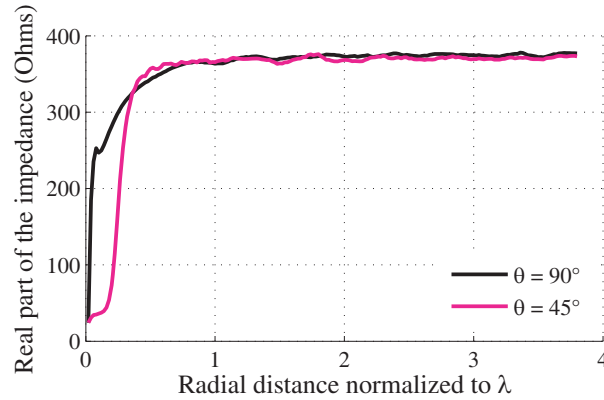
Figure 2. Real part of the wave impedance for a 0.46λ-dipole antenna of diameter equal to 5 mm operating at 2.45 GHz for free space conditions.

that the limit $2D^2/\lambda$ can be used safely to determine where the far field starts does not hold in general for all antennas. The analysis derived for any antenna radiating over free-space in [29] demonstrates that such a limit is valid only for larger antennas having their maximal dimensions at least equal to 5λ, which is clearly not the case for the presented example.

A setting that is of interest for WSNs is the location of antennas at different heights over a ground plane. In the following, we limit the analysis to ground plane with perfect electric conductor (PEC) characteristics. Of course, a more practical scenario arises when the surface of the ground plane introduces different electrical characteristics influenced by the type of soil and depth of penetration resulting in an effective permittivity and conductivity of a particular surface. Given the significant impact of such practical conditions on radio propagation, the analysis deserves a wide study that goes beyond the scope of this paper. Here, we consider a 0.46λ-dipole antenna located at different vertical distances from the plane surface, h. The cases of study are for different antenna heights (5, 9, 15 and 68 cm) above the ground plane. Fig. 3 plots the real part of the wave impedance as a function of the normalized distance.
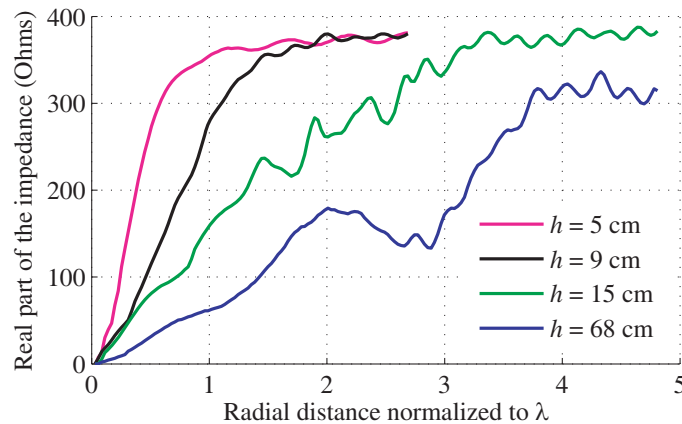

Figure 3. Real part of the wave impedance for a 0.46λ-dipole antenna of diameter equal to 5 mm operating at 2.45 GHz located above a PEC ground plane.

EM fields were computed by numerical simulation at several radial distances from the center of the antenna to a set of points chosen over a horizontal line (i.e., $\theta = 90°$). Fig. 3 shows a wave impedance equal to zero for the closest point to the antenna and for all the heights analyzed. This is a result of the relatively close proximity of the antenna with the ground plane which reduces the θ component of the resulting magnitude of the electric field vector. At larger radial distances, the wave impedance exhibits

different variations which are affected by the proximity of the antenna to the ground plane.

It is worth noting that oscillations presented in all curves are due to small scattering waves created by reflections with absorption boundaries, which are set well in the far-field region but rendering radial distances limited by a spheroidal boundary condition. Therefore, the numerical technique of the 3D field solver necessarily poses a level of inaccuracy when determining the far field onsets by comparing the computed impedance against the theoretical wave impedance.

Now, it is apparent that the cases of antennas with larger heights above the ground plane, the onset of the far field condition, which is effectively the approximation of the wave impedance to 120π, is reached at larger distances, in agreement with the analysis in [28]. For instance, for the 0.46λ-dipole antenna located at 5 and 9 cm over the PEC ground plane, the far field criterion is met at a distance approximately equal to 1.5λ and 2.5λ, respectively. In both cases, the far field condition is reached below the maximal distance displayed (2.7λ, see Fig. 3) showing little oscillation in the computed wave impedance around the characteristic impedance value. For this reason simulations were not conducted far away 2.7λ. For an antenna located at 15 cm, the onset of the wave impedance is located approximately at a distance of 4λ. In contrast, the case of the antenna located at 68 cm corresponds to the region defined by a radial distance (lower than 5λ) where the fields still create a complex near field scenario.

It is worth mentioning that there are other criteria that must be satisfied simultaneously to delineate the far field region from the near field [28, 29]. Here, for the sake of simplicity, the dipole antenna is only analyzed using the wave impedance criterion which determines the far field zone at which the power density vector is a real quantity. From a perspective of antennas for WSNs, this criterion covers a significant importance for power efficient devices.

Finally, it is worth mentioning that the far field conditions naturally could be different from those previously shown depending on the type of antenna. Antennas for WSNs are designed by taking into account the functional characteristics of the physical layer defined in the Standard IEEE802.15.4 [16, 17] and some particularities of wireless sensor networks exposed in Section 2. All the above have led to considering that antennas for WSNs have to achieve suitable impedance matching over specified bandwidths in compliance with the standard thus keeping acceptable power efficiencies of wireless devices. On the other hand, the antenna gain is chosen according to several considerations regarding the orientation between nodes. Near-isotropic antennas become a power efficient solution when network nodes are distributed uniformly (see for example [31]). Contrariwise, directional antennas present advantages in scenarios where obstructions create electromagnetic shadows between transmitter and receiver, thus radiation over these areas results in a waste of power [32]. Hence, the far field determination for these antennas and other designs proposed in the literature (much of these based on low-cost planar technology) is an important issue to be taken into account.

6. GROUND REFLECTION

Once fundamentals of free space and far field conditions have been addressed, we are in position to consider another propagation mechanism involved in wireless sensor networks. For outdoors communications, it is very common to find reflecting objects near LOS paths. This is the case revised here for the particular conditions of WSNs, where we shall specifically consider relatively short distances between terminals; in such a way the Earth's curvature can be neglected (i.e., it can be taken as a flat surface). It is worth noting that all equations related to components of electromagnetic fields and those derived from these in this section are valid for far field conditions as exposed in Section 5.

Then, from the aforementioned conditions, there are two media separated by a certain physical surface and the received signal results from a combination of a direct wave with length r_1 and a ground reflected wave with length r_2 as represented in Fig. 4 (hence its mathematical model is also known as *two-ray model*). It is worth noting that this surface can be regular or irregular in the sense of its dimensions and irregularities relative to the wavelength. It is said that there is a *specular reflection* if surface is large and that its irregularities are smaller than the wavelength (a smooth surface), or a *diffuse reflection* otherwise (i.e., considering a rough surface).

In any case, the amplitude and phase of the ground reflected wave are related to a parameter named *reflection coefficient*, ρ, which depends on the polarization of the wave, the dielectric constant of the
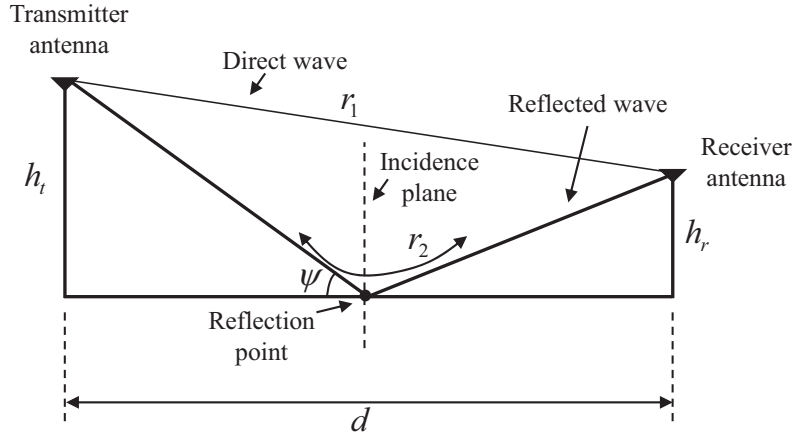
Figure 4. Geometry for the two-ray model. Adapted from [18].

medium relative to that of free space, $\varepsilon_r = \varepsilon/\varepsilon_0$, the conductivity of material, σ, where the radio wave is being reflected, and the incident angle of the wave respect to the surface, ψ. Thus, the reflection coefficients for horizontal (ρ_h) and vertical (ρ_v) polarizations are, respectively [18],

$$\rho_h = \frac{\sin\psi - \sqrt{(\varepsilon_r - jx) - \cos^2\psi}}{\sin\psi + \sqrt{(\varepsilon_r - jx) - \cos^2\psi}} \tag{15}$$

$$\rho_v = \frac{(\varepsilon_r - jx)\sin\psi - \sqrt{(\varepsilon_r - jx) - \cos^2\psi}}{(\varepsilon_r - jx)\sin\psi + \sqrt{(\varepsilon_r - jx) - \cos^2\psi}} \tag{16}$$

where $x = \sigma/\omega\varepsilon_0$, with ω the angular frequency, i.e., $\omega = 2\pi f$. As can be seen from Equations (15) and (16), for values of near-grazing incidence angle ($\psi \to 0$), reflection coefficients for both polarizations are equal to 1 in magnitude with a phase of $-180°$. As this angle increases, the magnitude and phase for ρ_h and ρ_v present certain trends depending upon distinct characteristics of ground and operational frequencies. In the case of horizontal polarization, for instance, the magnitude of ρ_h simply is less than 1, and its phase is reduced as well, both with an almost linear behavior. Regarding the reflection coefficient for signals with vertical polarization, it is more sensitive to variations of ψ provided that the electric field **E** is parallel to the plane of incidence and perpendicular to the reflecting surface. As ψ is increased, the magnitude of ρ_v is reduced up to a minimum value (for which the incidence angle is known as *Brewster angle*), and then it begins to increase again in an asymptotic form, whereas its phase approaches to zero (see [18] for some graphical examples).

Let E_d be the magnitude of the electric field associated to the direct wave. Then, the total magnitude of the received field, E, due to contributions of both direct and reflected waves can be expressed as

$$E = E_d\left[1 + \rho e^{-j\Delta\varphi}\right] \tag{17}$$

Provided that the reflection coefficient can be represented in terms of its modulus and its phase, ϑ, as $\rho = |\rho|\exp(j\vartheta)$,

$$E = E_d\left[1 + |\rho|\,e^{-j(\Delta\varphi - \vartheta)}\right] \tag{18}$$

In Eqs. (17) and (18) $\Delta\varphi$ represents the phase difference between the direct and reflected waves given by,

$$\Delta\varphi = \frac{2\pi}{\lambda}\Delta R \tag{19}$$

with ΔR the difference of paths lengths r_2 and r_1. From geometry of Fig. 4, it can be demonstrated that

$$\Delta R = d\left[\sqrt{1 + \frac{(h_t + h_r)^2}{d^2}} - \sqrt{1 + \frac{(h_t - h_r)^2}{d^2}}\right] \tag{20}$$

which for $d \gg h_t$, h_r can be approximated by

$$\Delta R = \frac{2h_t h_r}{d} \tag{21}$$

As exposed in Section 2, devices of WSNs can be located in diverse forms, following a specific deployment or in a random fashion for some cases where access is difficult. Their heights can vary from ground level up to some meters, and the ranges of radio links between nodes are at most 100 m. These peculiarities imply that in some applications h_t and h_r could be in the same order of d. In order to observe the approximation degree of Equation (21) for these scenarios, Fig. 5 shows a comparative example of plots for Equations (20) and (21), when $h_t = 1\,\mathrm{m}$ and $h_r = 1\,\mathrm{m}$, which can be practical heights in WSNs, and a distance up to $d = 10\,\mathrm{m}$. As can be appreciated, Equation (21) can be taken as a good approach to the original expression. Naturally, considerations should be taken for different values of h_t and h_r.
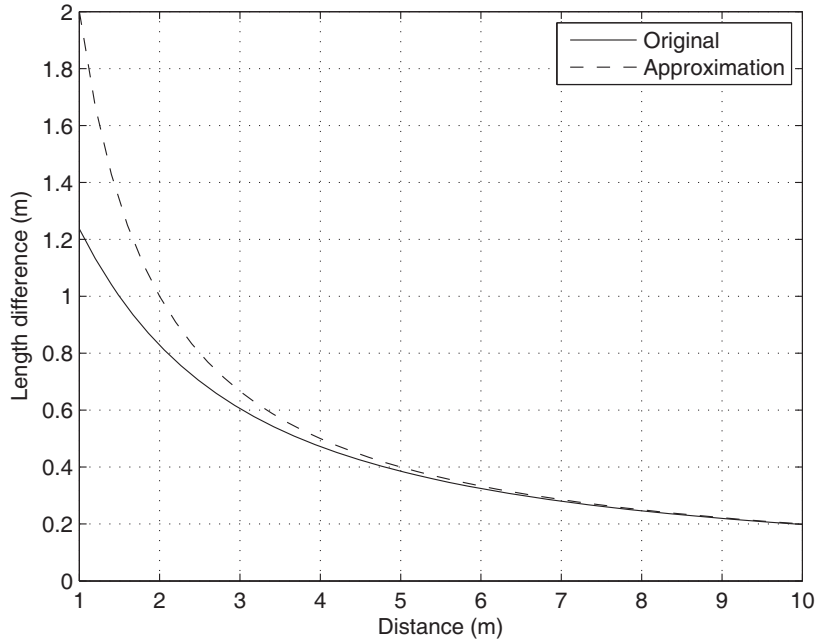

Figure 5. Length difference between r_2 and r_1 using the original expression given by (20) and the approximation of (21), both for $h_t = h_r = 1\,\mathrm{m}$.

Now, as has been seen, the magnitude of the total electric field is a function of the reflection coefficient, which in turn depends on the incidence angle, among other variables aforementioned. In this concern, it is important to review the behavior of ψ for WSNs. This angle depends on the position of the reflection point and therefore the antenna heights and their separation. A common way to determine the reflection point is by taking an image height of both antennas as depicted in Fig. 6 and by connecting them with the other antennas. The crossing point at the ground can be taken as reflection point.

From geometry of Fig. 6 it is straightforward to determine the incidence angle as $\psi = \arctan[(h_t + h_r)/d]$. Thus, different incidence angles were calculated for distinct combinations of antennas heights, when they are 10 m and 50 m separated (see Figs. 7(a) and 7(b), respectively). Results indicate that for relatively short distances, moderate values of ψ are present, and the assumption of $\psi \rightarrow 0$ can be valid only for relatively large antenna separations.

For the sake of simplicity, let us assume that $\psi \rightarrow 0$ such that $\rho = -1$ for both polarizations. In this way,

$$\begin{aligned} E &= E_d \left[1 - e^{-j\Delta\varphi} \right] \\ &= E_d \left[1 - \cos \Delta\varphi + j \sin \Delta\varphi \right] \end{aligned} \tag{22}$$
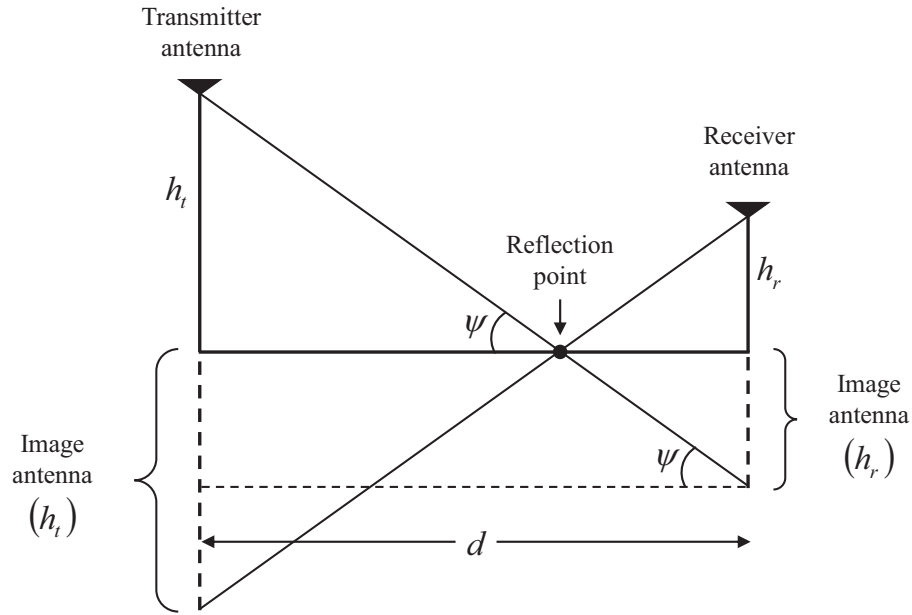
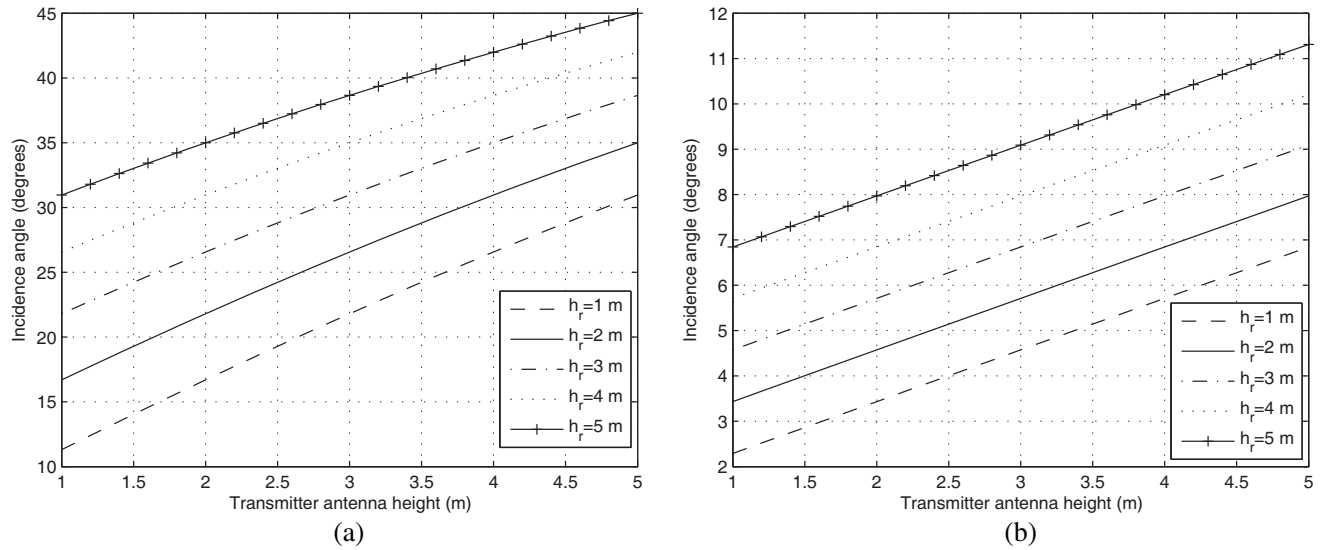**Figure 6.** Geometry to determine the incidence angle.

Figure 7. Incidence angle for different antennas heights and a separation of antennas: (a) $d = 10$ m, (b) $d = 50$ m.

Thus, by applying some well-known identities and substituting Equation (19), with the approach given in Eq. (21) into Eq. (22), the magnitude of E can be determined as

$$|E| = |E_d| \sqrt{1 + \cos^2 \Delta\varphi - 2\cos\Delta\varphi + \sin^2 \Delta\varphi}$$

$$= 2|E_d| \sin\frac{\Delta\varphi}{2}$$

$$= 2|E_d| \sin\left(\frac{2\pi h_t h_r}{\lambda d}\right) \tag{23}$$

Then,

$$P_r = 4\left|E_d\right|^2 \sin^2\left(\frac{2\pi h_t h_r}{\lambda d}\right) \tag{24}$$

Provided that the term $\left|E_d\right|^2$ corresponds to the received power of the direct LOS wave, it can be equal to Eq. (14). Therefore,

$$P_r = 4 P_t G_t G_r \left(\frac{\lambda}{4\pi d}\right)^2 \sin^2\left(\frac{2\pi h_t h_r}{\lambda d}\right) \tag{25}$$

The sine function in Equation (25) introduces variations in the amplitude of power due to the phase shift by the combination of the direct and reflected waves. Its variation on the received power can be graphically seen in Fig. 8, where different plots of P_r are depicted (in dBm) using a normalized transmitted power $P_t = 1\,\text{mW}$, isotropic antennas ($G_t = G_r = 1$), an operational frequency of $2.4\,\text{GHz}$, and three cases of antenna heights. As can be observed, a pattern of nulls is formed, which, following the free space profile, produces multiple crossings with it. The rate and depth of these nulls are related to the antennas heights, and they are observed up to a point where crossings are not longer present. Basically, before this crossing a power decay law with the distance of $20\,\text{dB}$ per decade is present, whereas a slope of $40\,\text{dB}$ per decade is the trend after this last crossing. It is worth mentioning that Equation (25) and therefore results of Fig. 8 are valid only for far field conditions as we have already stated at the beginning of this section. However, please note that the assumption of isotropic antennas was only for the sake of simplicity in order to show the behavior of the model, but it does not have meaning for this non-physical antenna.
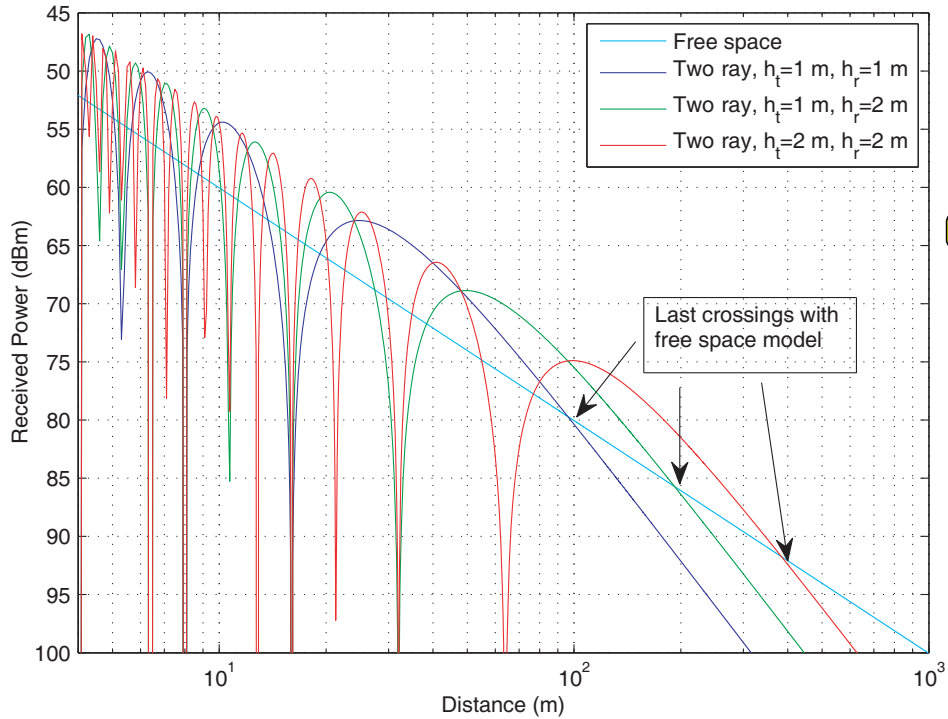

Figure 8. Received power for the two-ray model.

7. TWO-SLOPE MODEL

From the two propagation models addressed in Sections 4 and 6, it is clear that there exists a dependence on the received power with the distance between wireless terminals. This dependence is related with what is known as *power decay exponent* or *path loss exponent*, γ, which represents the slope of the

corresponding curve that characterizes a particular model. In other words, γ denotes the power-law relationship between the separation distance and the receiver power. Thus, we can see that for the free space model, $P_r \propto 1/d^2$, in such a way that $\gamma = 2$, whereas for the two-ray model, two slopes can be appreciated with $\gamma = 2$ before the last crossing with the free space model and $\gamma = 4$ beyond. For this reason, it is considered as a *two-slope model*.

It is worth mentioning that the path loss exponent could experimentally present different values depending on the environment where the wireless terminals are deployed. For example, a comparison between 1.8 GHz measurements and simulations was carried out by Prasad et al. [33] in urban, dense urban, and suburban areas. According to their observations, γ takes values between 3 and 4 for distances between 200 and 500 m depending on the location under consideration. On the other hand, in [34] measurements were conducted in an environment of underground mines for LOS and NLOS (non-LOS) conditions, in a range from 1 to 10 m, using different combinations of omni and directional antennas for the transmitter and the receiver. From the experimental data the authors determine γ through a linear regression analysis. For LOS case, values very close to 2 were obtained, whereas for NLOS, larger values of 3 and 6.16 resulted. For an indoor environment the propagation on stairwells was studied for applications where these are important in an emergency situation [35]. Measurements were conducted at 2.4 and 5.8 GHz in the premises of the University of Hawaii. Values of γ as high as 8.3 and 9.74 are found for these frequency bands, respectively.

In the case of two-slope model, the distance where the slope changes is determined by equaling Equations (14) and (25). In general terms, this distance, named *breakpoint distance*, d_{bp}, is a function of the antennas heights and the wavelength. At this regard, there are several approaches to determine this distance. For example, a well-known approach is based on the principle of the first Fresnel ellipse clearance, for which the breakpoint distance corresponds to the point where the ground reaches the first Fresnel zone[†], as depicted in Fig. 9, and results as [12]:

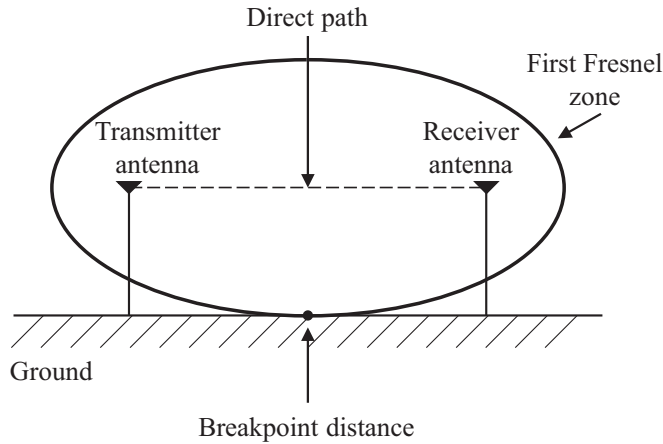$$d_{bp} \approx \frac{4h_t h_r}{\lambda} \tag{26}$$

Figure 9. Determination of the breakpoint distance from the first Fresnel zone.

Although it can be found in the open literature some expressions to calculate this distance (see Table 1 for instance), it has been pointed out by some authors that a single distance is sometimes difficult to be determined, and a "transition region" between the two slopes can be identified instead. In this situation, a double regression analysis is carried out from experimental data. From diverse experiments, Green exposes that this distance can be bounded by [38]

$$\frac{\pi h_t h_r}{\lambda} < d_{bp} < \frac{4\pi h_t h_r}{\lambda} \tag{27}$$

[†] *"A Fresnel zone is the circular portion of a wavefront transverse to the line between the source and a point of observation, whose centre is the intersection of the front with the direct ray and whose radius is such that the shortest path from the source through the periphery to the receiving point is one-half wave longer than the ray."* [37].

Table 1. Expressions for the breakpoint distance.

Reference	Model
[38]	$\frac{2\pi h_t h_r}{\lambda}$
[39]	$\frac{4h_t h_r}{\lambda}$
[40]	$\frac{8.41 h_t h_r}{\lambda}$

In the context of WSNs, the two-ray two-slope model has been adopted by some authors (see [20] and references therein), using $\gamma = 2$ before d_{bp} and $\gamma = 4$ beyond. However, as Foran et al. state [41], if antennas are very near the ground, this model could not present enough accuracy. In fact, Feuerstein et al. suggest that several wavelengths or more above the horizontal ground plane should be taken as threshold for the antennas heights in order to use the two-ray model [42].

8. DIFFRACTION

The diffraction phenomenon is commonly present in different radio wave propagation environments, characterized by the fact that an obstacle can be found into the direct path between terminals or relatively near it as depicted in Fig. 10. According to the geometry of this figure, relative position of terminals and obstacle play an important role in the diffraction phenomenon. The closer the receiver is to the obstacle, the larger the diffraction losses will be experimented in the radio wave propagation [36]. In this concern, nodes of WSNs deployed for applications under ground could be exposed to this situation, where the "obstacle" would be the ground. For example, for some applications of WSNs over ground but relatively near it, the effect of the surface characteristics and the antennas height is studied in [21]. The authors found that the path loss exponent is affected by these conditions. Values of this exponent between 1.70 and 2.27 are obtained for an antenna height of 50 cm, whereas for an antenna height of 9 cm the path loss exponent increases between 2.90 and 3.4 [21]. Thus, the closer the antenna is to the surface, the shorter the node range is, which is attributed to the obstruction of ground to the transmission path.
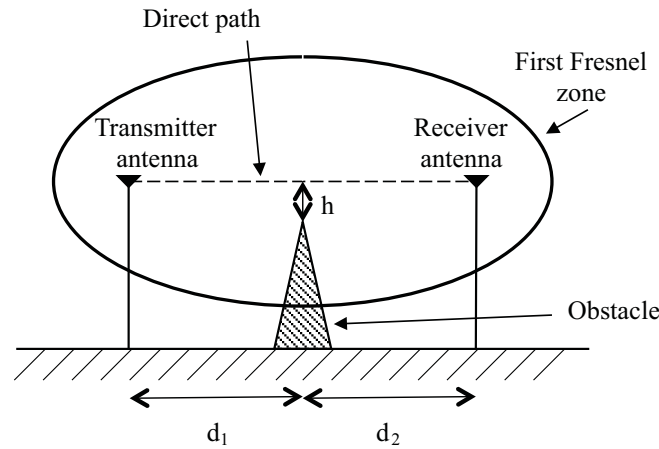
Figure 10. Geometry of the knife edge obstacle in the first Fresnel zone.

Recently, modeling based on diffraction theory for near-ground channel in WSNs has been published [12], with good results compared to independent measurement campaigns. Basically, Torabi and Zekavat define three propagation regions derived from a geometry where antennas are at relatively low height as can be found in some applications of WSNs [12]:

- *Short-range communication*: The first Fresnel zone is clear of obstacles and is delimited by the breakpoint distance, for which the exact formulation is used instead of the classical

approximation (26) taken from microcellular mobile systems:

$$d_{bp} = \frac{4h_t h_r}{\lambda} \sqrt{1 - \frac{\lambda^2(h_t^2 + h_r^2)}{(4h_t h_r)^2} + \left(\frac{\lambda^2}{16h_t h_r}\right)^2} \tag{28}$$

- *Medium-range communications*: The first Fresnel zone tangentially touches the ground surface as in Fig. 9. In this case, diffraction begins to take importance, and it is possible to define this region lower bounded by Eq. (28) and limited up to a "critical distance" given by:

$$d_c = \sqrt{\left(\frac{12.5h_t h_r}{\lambda} - \frac{\lambda}{12.5}\right)^2 - (h_t - h_r)^2} \tag{29}$$

The electromagnetic obstruction of the first Fresnel zone, introduced by the closeness of antennas to the ground, produces an excess loss factor (relative to that of free space), L_{ex}, given by

$$L_{ex} = \left| 1 + \frac{r_1}{r_2} \rho^{ef} e^{-j\Delta\varphi} \right|^2 \tag{30}$$

Please note that r_1 and r_2 correspond to the direct and reflected paths, respectively, as depicted in Fig. 4, and $\Delta\varphi$ represents its phase difference as explained in Section 6. The term ρ^{ef} is defined in [12] as an effective reflection coefficient, which, as the authors claim, stands for the "surface" waves (see Section 9 below), incident polarization and surface correlation length, whose analysis is valid for low-grazing incident angles as the case at hand. See [12] and references therein for details on the derivation of ρ^{ef}.

- *Long-range communications*: For antenna heights lower than those which satisfy conditions of medium-range communications, a significant part of the first Fresnel zone is always occupied by the ground, in such a way that the link range exceeds d_c. In this case, Torabi and Zekavat [12] claim that the total path loss is given by the knife edge diffraction loss, L_{ke}, that assumes an asymptotically thin diffracting obstruction at the middle of the path,

$$L_{ke} = \left[0.5 + \frac{0.877(h_t + h_r)}{\sqrt{\lambda d}} \right]^2 \tag{31}$$

and an additional loss, given by L_{ex} in Eq. (30), accounts for rough terrain parameters such as permittivity and roughness statistics introduced in ρ^{ef}.

Thus, the proposal of [12] for a path loss model (in dB) of WSN under near-ground conditions is:

$$L_{NG} = \begin{cases} L_{fs}; & d \leq d_{bp} \\ L_{fs} + L_{ex}; & d_{bp} \leq d \leq d_c \\ L_{fs} + L_{ex} + L_{ke}; & d \geq d_c \end{cases} \tag{32}$$

with L_{fs} the corresponding free space path loss. In Eq. (32), we present the limits as given in the original reference, although according to its derivation it could be

$$L_{NG} = \begin{cases} L_{fs}; & d \leq d_{bp} \\ L_{fs} + L_{ex}; & d_{bp} < d \leq d_c \\ L_{fs} + L_{ex} + L_{ke}; & d > d_c \end{cases} \tag{33}$$

9. SURFACE WAVES

Provided that several applications of WSNs require nodes are very near the ground surface (e.g., traffic monitoring for intelligent transport systems [43]), it is important to review the topic of electromagnetic fields at the Earth's surface.

9.1. Origins and Fundamentals

The subject of surface waves has been studied since the very early stages of radio communications, which took importance when it was assumed that propagation of radio waves following the Earth's curvature was the mechanism to explain the success of the transatlantic communication experiment of Marconi (in those years the ionospheric layer was unknown). Before this date, the name of *surface waves* had already been coined by Lord Rayleigh to refer to some radio waves propagating along the interface between two media [44]. Years later, the famous 1909 work by Sommerfeld [45] was published addressing a solution to the effect of the finite conductivity of the ground on the radiation from a short vertical antenna at the surface of a plane Earth. An interesting result derived from his work is that the Hertzian vector Π related to the total electromagnetic field considering both media, air and ground, can be divided in two components: $\Pi = \Pi_1 + \Pi_2$, where Π_1 represents the contribution of the "space" wave, and Π_2 the corresponding part of a "surface" wave (afterwards, these terms were specified by diverse authors, e.g., [44], as a direct wave from the source and a superposition of waves resulting from the phenomena of reflection on a surface and refraction through a surface, respectively). During several decades, controversy arose about the Sommerfeld's formulation (partially by the fact that an average ground, with $\sigma = 5 \times 10^{-3}$ Siemens and $\varepsilon_r = 15$, cannot be considered neither conductor nor dielectric [36]), and different definitions for surface wave were considered as pointed out by [22, 44, 46, 47].

It is important to mention that the timely paper of Sarkar et al. [22] presents a very useful survey from a historical, physical, mathematical, and practical points of view on the matter of surface waves. One of the aspects addressed there is the analysis of diverse approaches generated by several authors and how different definitions of surface wave were addressed. Thus, in an important effort to clarify this confusion an emphasis is given there what authors name as *true* surface waves in the Rayleigh sense as explained by Schelkunoff [44]. In what follows the properties and fundamentals of true surface waves shall be addressed, and the term known as Sommerfeld's surface waves shall be pointed out only where it corresponds.

Let us now review some fundamentals of surface waves. The nature of these waves can be explained by the change from free space conditions (where the waves are spherical) to a scenario of plane or cylindrical waves caused by the introduction of a plane perpendicular to a vertical antenna [48]. In the former case, the amplitude of the waves varies inversely as the distance, whereas for the latter it varies inversely as the square root of the distance. This "reduction" in the amplitude of the waves seems to indicate that a portion of the wave is altered by the presence of the plane surface. In this way, the generation of plane or cylindrical waves can be achieved by the presence of a type of "wave guide", which is the physical explanation given by Sommerfeld to the surface waves [48]. Nevertheless, the fields associated with these waves present an evanescent nature, which is remarkable at upper heights from the planar boundary, whereas the wave is more concentrated on this plane as the frequency is increased, and as a consequence, its evanescent nature is also dependent on frequency [52].

Another approach on the subject is addressed by Schelkunoff, who exposes, in a simple way, the physical fundamentals of surface wave propagation [44], which is centered in the reflection and refraction principles[‡]. As explained in Section 6, there exists the Brewster angle, corresponding to the incidence angle where the magnitude of the reflection coefficient for a vertical polarized wave is minimum. At this angle, there is not reflection, and the total refraction is present in such a way that it seems that the wave is trapped by the ground.

It is worth mentioning the work of Norton [46], who also states that a particular property that identifies to a surface wave is its predominance near the surface of the Earth provided that at larger heights, it becomes negligible, and the total field is dominated by the space wave. The physical meaning given by Norton to the Poyting vector derived from the his formulation is that the energy flows downwards toward the ground in such a way that ground currents are induced. Thus, one could relate this behavior to the total refraction phenomenon. However, as pointed out in [52] this phenomenon is independent of frequency, hence provided the nature of surface waves, they cannot be associated with it.

These issues are summarized in the monograph presented by Barlow and Brown [49], where different aspects of the surface waves are addressed, like conditions for supporting this waves at an interface

---

[‡] Sometimes it is said that a radio wave is *transmitted* from a medium to another one, when it is propagating by a refraction mechanism.

between two different media, the power carried by them, the relationship of the Brewster angle with these waves, analysis for different surfaces, etc. Basically, the authors state that these waves propagate *without radiation* along an interface between two different media, with this interface being the surface that supports them. In order to fulfill this condition, the interface must be straight in the direction of propagation, although it is not necessarily in the transverse direction [49]. The peculiarity that the surface acts as a physical mechanism to support these waves allows them to be also referred as *guided waves*.

9.2. Absence of Surface Waves

As already mentioned, different analyses have been carried out by diverse authors in the surface waves subject. These include theoretical and experimental results which we recommend [51] for more details. Here we consider a couple of approaches whose theoretical results show the absence of the surface waves. Latter, we outline some experiments presented by some authors that confirm these conclusions.

Then, let us start with the work of Bremmer [50] who considers a multipath environment from the transmitter to the receiver, where surface waves are included. He centers his analysis about surface waves in terms of its phase velocity. It is given by c/n_{12}, where n_{12} is related with the refractive indexes of both media, n_1 and n_2, and is defined as

$$\frac{1}{n_{12}^2} = \frac{1}{n_1^2} + \frac{1}{n_2^2} \tag{34}$$

These terms are introduced in the mathematical analysis given by Bremmer [50] for the Hertzian vector Π, where arbitrary conditions of the vertical positions of dipole used as transmitter are included. The expressions given for Π consider direct wave, earth-refracted wave, and surface wave.

Thus, Bremmer carries out an impulse response analysis which indicates that those components associated with surface waves could be presented before the arrival of the main pulse (i.e., in the transient period) in such a way that they are canceled by mutual interference. Moreover, he states that this cancelation is presented in that region that the waves coming from the source reach the receiver via reflection and refraction in directions less steep than the Brewster angle, and therefore it implies the absence of surface waves.

Let us now take the approach based on the reflection coefficient involved in the Hertzian vector in the Sommerfeld's solution. In order to address this issue, three papers [22, 51, 52] complementary each other are considered here as the basis of explanation. Then, from the expression of Hertzian vector that satisfies wave equations and boundary conditions for a vertical electric dipole located at (x', y', z') over a plane surface at $z = 0$, Π_z is given by [51],

$$\Pi_z = P \left\{ \frac{\exp(-jk_1 R_1)}{R_1} + \int_0^\infty \frac{J_0(\xi d_{xy})}{\sqrt{\xi^2 - k_1}} K(\xi) \exp\left[-\sqrt{\xi^2 - k_1^2}(z + z')\right] \xi \, d\xi \right\} \tag{35}$$

for $\text{Re}(\sqrt{\xi^2 - k_1^2}) > 0$. The first term between brackets of Eq. (35) represents Π_1, i.e., the solution due to the contribution of the direct wave, whereas the integrand term corresponds to Π_2, in this case the solution to the contribution of the superposition of waves caused by the phenomenon of reflection on the plane surface. Now, $J_0(\cdot)$ is the zero order Bessel function of first kind, k_1 the propagation constant in the air, i.e., $k_1 = \omega\sqrt{\mu_0 \varepsilon_0}$ (which is related to the propagation constant of ground plane by $k_2 = k_1 \sqrt{\varepsilon}$), $d_{xy} = \sqrt{(x - x')^2 + (y - y')^2}$, $R_1 = \sqrt{d_{xy}^2 + (z - z')^2}$, and ξ the variable of integration. The parameter P is given by

$$P = \frac{I dz}{j\omega 4\pi \varepsilon_0} \tag{36}$$

with $I dz$ the dipole moment of the elementary current. In Eq. (35) the function $K(\xi)$ is expressed by

$$K(\xi) = \frac{k_2^2 \sqrt{\xi^2 - k_1^2} - k_1^2 \sqrt{\xi^2 - k_2^2}}{k_2^2 \sqrt{\xi^2 - k_1^2} + k_1^2 \sqrt{\xi^2 - k_2^2}} \tag{37}$$

for $\mathrm{Re}(\sqrt{\xi^2 - k_2^2}) > 0$. This function corresponds to the reflection coefficient[§] from which the Brewster angle is related to its zeros, and its poles are associated with the surface wave. By following the formulation found in [22] and [51], on the one hand, the actual location of the pole in the complex plane is not as given by Sommerfeld, and on the other hand, the branch cut contour can be chosen in such a way that the contribution of the pole is excluded. Thus, the absence of such waves is theoretically confirmed.

Regarding some experimental results found in the open literature, the measurements reported by Burrows are a classical reference in the context of propagation over plane earth and its relationship to surface waves [53]. These measurements were conducted over a fresh water calm lake of great depth (in order to be considered as a quasi-flat surface) at 150 MHz for distances from 1 m to around 2 km with antennas heights around 0.5 m. Then, results were also obtained by considering different combinations of antennas heights, and specifically, two sets of measurements were recorded, the first one when the transmitter is at 2.5 m height and the second one for a 24.8 m height. From his results he did not find any evidence of a component related to the surface wave as theoretically formulated by Sommerfeld.

Finally, Jeon and Grischkowsky [54] present results for a THz pulse propagating over an Aluminum sheet, whose source is very near it (the order of millimeters). The authors report a reduction from 34 pA to 5.1 pA in the amplitude of the peak-to-peak pulse measured from a distance of 14 cm to 98 cm, respectively. This reduction implies a path loss exponent of 2 provided the quadratic relationship between amplitude and power (see Section 4), which is translated to a spherical waves behavior. Hence, it does not present the surface waves features.

Thus, the results reported by [53, 54] experimentally show the absence of surface waves, which is of particular interest for WSNs as indicated at the beginning of this section. This has been shown even for very short distances, relatively high frequencies, and antennas very close to a surface as can be seen in [54].

10. ATTENUATION DUE TO VEGETATION

Some applications of wireless sensor networks, like precision agriculture and prevention of forest fire, are typical examples in which wireless devices are obviously in a vegetation environment either trees, plants, grass, etc. (see [7, 55–57]). In this context, for instance, an experimental study has been conducted considering a deployment of a WSN in a forest where the influence of the trunks in the received power by means of a linear regression model has been analyzed [55]. Another study in this direction is presented by Tokunou et al. [56] for a WSN in a forest environment with antennas height set at 105 cm. According to their measurement results, it seems that a notches pattern can be identified in the relationship between received signal strength and distance, which can be associated with the two-ray model described in Section 6.

On the other hand, in some occasions the scenario where a WSN is deployed can be near or inside a region of relative vegetation (residential zones, university campuses, parks, crop fields, etc.). For example, in [57] a model to determine the topology of a WSN is proposed for crop fields. The baseline in this work is that for precision agriculture, where some parameters have to be monitored like temperature, humidity, soil moisture content, among others, nodes are exposed to the grown of vegetation under analysis, so propagation scenario can be modified as a function of the time. Thus, based on the fact that crop fields usually follow a regular grid, it is possible to consider a statistically uniform distribution of scatters and assume that the line of sight paths can be formed to the sink node (where information is collected), so Equation (14) can be taken for simulations [57]. However, it is important to note that some radio waves could reach the sink node via other propagation paths for which more sophisticated propagation models should be considered.

Then, the importance to review this topic is that all types of vegetation conserve certain quantity of humidity depending on the age and spice, through which some currents are induced, and as a consequence, an attenuation effect is present due to absorption and scattering [58]. In this context, the effect of vegetation encroachment on a WSN is studied in [59] where a monitoring system for measuring vegetation around transmission power lines is proposed. There, it is observed that the larger

---

[§] Please note that in the case of Equation (16), the reflection coefficient is for a specular wave, whereas Eq. (37) is for a superposition of a bunch of waves [51].

the vegetation encroachment is, the lower the received power level is by nodes at a specific separation distance.

In addition, the density of vegetation and operational frequency are factors that can be related to this attenuation. The Inform 236–6 of the CCIR [60] outlines a set of studies carried out on this topic during the 1950 decade, although it was presented mainly for relatively long paths. Years later, Weissberger presented an extensive report of measurements for predicting the attenuation due to trees and underbrush in a wide span of frequencies at template latitudes (dense, dry, and in-leaf trees) with distances up to 400 m [61], which can be suitable for WSNs. His results have been cited by different authors for research in diverse applications (see [62–66] for instance). Based on his observations, Weisberger proposed what is known as *Modified Exponential Decay* (MED) model, which determines the losses in excess (in dB) relative to that of free space as a function of the operational frequency in GHz, f_{GHz}, and the foliage depth in m, d_f as

$$
L_{tree} = \begin{cases} 1.33 \, f_{\text{GHz}}^{0.284} \, d_f^{0.588}; & 14 \leq d_f \leq 400 \\[2mm] 0.45 \, f_{\text{GHz}}^{0.284} \, d_f; & 0 \leq d_f < 14 \end{cases} \tag{38}
$$

In 2010, Kamarudin et al. [58] and Gay-Fernández et al. [55], followed by Mestre et al. [13] in 2011, and Sabri et al. [67] in 2013 published studies of radio wave propagation through vegetation for WSNs scenarios. From these, the work of Mestre et al. results in practical interest because they present a revision of propagation models candidate for the standard IEEE802.15.4. Basically, the total losses proposed in [13] are

$$
PL_{tot} = A + \alpha A_{model} \tag{39}
$$

where A denotes the path loss of a certain model without considering the vegetation effect, A_{model} the attenuation given by a specific vegetation model, and α is simply a multiplicative factor,

$$
\alpha = \varrho\beta \tag{40}
$$

with ϱ the vegetation density ($0 \leq \varrho \leq 1$) and β an empirical constant depending on the vegetation type. It is worth mentioning that the authors bound their model as long as the used vegetation model follows an exponential decay profile like the Weissberger model.

In this concern, the problem of nonuniform vegetation (from a point of view of the spatial distribution of vegetation, age, spice and its combination with buildings) was recently addressed in [14]. In this study, the proposal given in Eq. (39) taking as base of Eq. (38) was explored for a WSN used for electric energy consumption monitoring. The authors used a Lidar database, which was of importance to account for the vegetation (this database provides relative heights of terrain, building and any object like trees). An overestimation of path loss was observed, which was attributed to the fact that nodes heights were under the foliage of some trees. To solve this situation, a "canopy threshold" was introduced in the determination of the path profile in such a way that only "significant" trees were considered. For the scenario under study, acceptable results were obtained. Additionally, Galvan-Tejada and Duarte-Reynoso [14] found that depending on the foliage density, signal could propagate via a diffraction mechanism over the trees canopies or through them.

Finally, in a recent publication [68], the effect of orientation of nodes is addressed for those applications where nodes are air-dropped into a large vegetation area. Specifically the authors consider jungle-like tree vegetation environments, where nodes could be at different orientations (upright, sideways, vertical-up, upside down, etc.) and positions (ground, tree trunk level, canopy, etc.), depending on how they fall. As Olasupo and Otero pointed out [68], this situation impacts on the levels of received power, which is corroborated with their empirical path loss models derived by curve fitting. These models are compared with classical models like Equation (38), for which some significant differences are found. Particularly, the authors claim that an underestimation of the path loss is introduced by classical model, therefore the importance of considering the nodes orientation. Nevertheless, a function that characterizes the probability of node orientation is not presented, which could be dependent on the vegetation spice and density. Hence, new studies are required in this field.

11. CONCLUSION

A revision of radio wave propagation for wireless sensor networks is presented in this paper. Classical topics like free space, far field, reflection, diffraction and surface waves are addressed from a theoretical point of view, where some considerations specific for these networks are pointed out. A key parameter is the height of antennas, which are usually located at low altitudes, from a few centimeters up to few meters depending on the application. In this concern, simulations were conducted for antenna heights very close to ground, and far field conditions were determined. We found that the characterization of far field needs larger distances when the antennas are located at higher heights above the ground plane. Attenuation due to vegetation is also related to this parameter, and although there are some works it, it is still an open theme. Rain attenuation is a further topic to be explored in the field of wireless sensor networks. Although it is a well characterized phenomenon, it has not been considered (mainly due to the typical frequencies where these networks are being developed). However, in some situations of heavy rainstorms for long time periods, its impact on the network performance is not negligible. Moreover, if a WSN is in a high density vegetation environment, rain attenuation could be a crucial factor.

REFERENCES

1. Mainwaring, A., J. Polastre, R. Szewczyk, D. Culler, and J. Anderson, "Wireless sensor networks for habitat monitoring," *02 Proceedings of 1st ACM International Workshop on Wireless Sensor Networks and Applications*, 88–97, September 2002.

2. Rashvand, H. F., A. Abedi, J. M. Alcazar-Calero, P. D. Mitchell, and S. C. Mukhopadhyay, "Wireless sensor systems for space and extreme environments: A review," *IEEE Sensors Journal*, Vol. 14, No. 11, 3955–3970, November 2014.

3. Zhai, X. and T. Vladimirova, "Data aggregation in wireless sensor networks for lunar exploration," *2015 Sixth International Conference on Emerging Security Technologies*, 30–37, Braunschweig, Germany, 2015.

4. Neuhold, D., J. F. Schmidt, C. Bettstetter, J. Klaue, and D. Schupke, "Experiments with UWB aircraft sensor networks," *2016 IEEE Conference on Computer Communications Workshops (INFOCOM WKSHPS): Student Activities*, 948–949, San Francisco, CA, USA, 2016.

5. Jiang, J., G. Han, C. Zhu, S. Chan, and J. P. C. Rodrigues, "A trust cloud model for underwater wireless sensor networks," *IEEE Communications Magazine*, Vol. 55, No. 3, 110–116, March 2017.

6. Ramson, S. R. J. and D. J. Moni, "Applications of wireless sensor networks — A survey," *2017 International Conference on Innovations in Electrical, Electronics, Instrumentation and Media Technology (ICEEIMT)*, 325–329, Coimbatore, India, 2017.

7. Lopez-Iturri, P., M. Celaya-Echarri, L. Azpilicueta, E. Aguirre, J. J. Astrain, J. Villadangos, and F. Falcone, "Integration of autonomous wireless sensor networks in academic school gardens," *Sensors*, Vol. 18, 3621, 1–18, 2018.

8. Palattella, M. R., M. Dohler, A. Grieco, G. Rizzo, J. Torsner, T. Engel, and L. Ladid, "Internet of things in the 5G Era: Enablers, architecture, and business models," *IEEE Journal on Selected Areas in Communications*, Vol. 34, No. 3, 510–527, 2016.

9. Chen, L. and C. Englund, "Choreographing services for smart cities: Smart traffic demonstration," *2017 IEEE 85th Vehicular Technology Conference (VTC Spring)*, 1–5, Sydney, NSW, Australia, 2017.

10. Osman, Z., S. N. Azemi, A. A. M. Ezanuddin, and L. M. Kamarudin, "Compact antenna design for outdoor RF energy harvesting in wireless sensor networks," *2016 3rd International Conference on Electronic Design (IECD)*, 199–202, August 2016.

11. Rahman, M. and J.-D. Park, "The smallest form factor UWB antenna with quintuple rejection bands for IoT applications utilizing RSRR and RCSRR," *Sensors*, Vol. 18, No. 911, 1–16, 2018.

12. Torabi, A. and S. A. Zekavat, "Near-ground channel modeling for distributed cooperative communications," *IEEE Transactions on Antennas and Propagation*, Vol. 64, No. 6, 2494–2502, June 2016.

13. Mestre, P., J. Ribeiro, C. Serodio, and J. Monteiro, "Propagation of IEEE802.15.4 in vegetation," *Proceedings of the World Congress on Engineering 2011*, Vol. II, 2011.

14. Galvan-Tejada, G. M., and E. Q. Duarte-Reynoso, "Some guidelines to simulate wireless sensor networks in a propagation environment with non-uniform vegetation," *International Journal on Sensor Networks*, Vol. 17, No. 1, 40–51, 2015.

15. Tavli, B., K. Bicakci, R. Zilan, and J. M. Barceló-Ordinas, "A survey of visual sensor network platforms," *Multimedia Tools Applications*, Vol. 60, No. 3, 689–726, October 2012.

16. 802.15.4-2011: IEEE Standard for Local and Metropolitan Area Networks. Part 15.4: Low-Rate Wireless Personal Area Networks (LR-WPANs), September 2011.

17. 802.15.4-2015: IEEE Standard Low-Rate Wireless Networks, December 2015.

18. Jordan, E. C. and K. G. Balman, *Electromagnetic Waves and Radiating Systems*, 2nd Edition, Prentice-Hall, Englewood Cliffs, NJ, 1968.

19. Boithias, L., *Radio Wave Propagation*, McGraw-Hill, New York, 1987.

20. Kurt, S. and B. Tavli, "Path loss modeling for wireless sensor networks," *IEEE Antennas & Propagation Magazine*, Vol. 59, No. 1, 18–37, February 2017.

21. Ndzi, D. L., M. A. M. Arif, A., Y. M. Shakaff, M. N. Ahmad, A. Harun, L. M. Kamarudin, A. Zakaria, M. F. Ramli, and M. S. Razalli, "Signal propagation analysis for low data rate wireless sensor network applications in sport grounds and roads," *Progress In Electromagnetics Research*, Vol. 125, 1–9, 2012.

22. Sarkar, T. K., W. Dyab, M. N. Abdallah, M. Salazar-Palma, M. V. S. N.Prasad, S. Barbin, and S. Weng Ting, "Physics of propagation in a cellular wireless communication environment," *Radio Science Bulletin*, No. 343, 5–21, December 2012.

23. Livingston, D. C., *The Physics of Microwave Propagation*, Prentice-Hall, Englewood Cliffs, NJ, 1970.

24. Seely, S., "Poynting's theorem and the energy-flow postulate," *Transactions on Education*, Vol. 27, No. 4, 246, November 1984.

25. Friis, H. T., "A note on a simple transmission formula," *Proceedings of the I.R.E. and Waves and Electrons*, 254–256, May 1946.

26. Balanis, C. A., *Antenna Theory: Analysis and Design*, 3rd Edition, Wiley-Interscience, Hoboken, NJ, 2005.

27. IEEE Standard 211–1997, "IEEE Standard Definitions of Terms for Radio Wave Propagation," *Wave Propagation Standards Committee of the Antennas and Propagation Society*, 1–43, December 1997.

28. De, A., T. K. Sarkar, and M. Salazar-Palma, "Characterization of the far-field environment of antennas located over a ground plane and implications for cellular communication systems," *IEEE Antennas and Propagation Magazine*, Vol. 52, No. 6, 19–40, December 2010.

29. Abdallah, M. N., T. K. Sarkar, M. Salazar-Palma, and V. Monebhurrun, "Where does the far field of an antenna start?," *IEEE Antennas and Propagation Magazine*, 115–124, October 2016.

30. Krauss, J. D., *Antennas*, 2nd Edition, McGraw-Hill, New York, 1988.

31. Farooqui M. F. and A. Shamim, "A 3D printed near-isotropic antenna for wireless sensor networks," *2016 International Symposium on Antennas and Propagation (ISAP)*, 94–95, Okinawa, Japan, October 24–28, 2016.

32. Michalopoulou, A., E. Koxias, F. Lazarikis, T. Zervos, and A. Alexandridis, "Investigation of directional antennas effect on energy efficiency and reliability of the IEEE 802.15.4 Standard in outdoor wireless sensor networks," *2015 IEEE 15th Mediterranean Microwave Symposium (MMS)*, 1–4, Lecce, Italy, November 30–December 2, 2015.

33. Prasad, M. V. S. N., S. Gupta, and M. M. Gupta, "Comparison of 1.8 GHz cellular outdoor measurements with AWAS electromagnetic code and conventional models over urban and suburban regions of Northern India," *IEEE Antennas and Propagation Magazine*, Vol. 53, No. 4, 76–85, August 2011.

34. Rissafi, Y., L. Talbi, and M. Ghaddar, "Experimental characterization of an UWB propagation channel in underground mines," *IEEE Transactions on Antennas and Propagation*, Vol. 60, No. 1, 240–246, January 2012.

35. Lim, S. Y., Z. Yun, and M. F. Iskander, "Propagation measurements and modeling for indoor stairwells at 2.4 and 5.8 GHz," *IEEE Transactions on Antennas and Propagation*, Vol. 62, No. 9, 4754–4761, September 2014.

36. Parsons, J. D., *The Mobile Radio Propagation Channel*, John Wiley & Sons, New York, 1992.

37. Dolukhanov, M., *Propagation of Radio Waves*, Mir Publishers, Moscow, 1971.

38. Green, E. and M. Hata, "Microcellular propagation measurements in an urban environment," *IEEE International Symposium on Personal, Indoor and Mobile Radio Communications*, 324–328, UK, 1991.

39. Xia, H. H., H. L. Bertoni, L. R. Maciel, A. Lindsay-Stewart, and R. Rowe, "Radio propagation characteristics for line-of-sight microcellular and personal communications," *IEEE Transactions on Antennas and Propagation*, Vol. 41, No. 10, 1439–1447, October 1993.

40. Perera, S. C. M., A. G. Williamson, and G. R. Rowe, "Prediction of breakpoint distance in microcellular environments," *Electronics Letters*, Vol. 35, No. 14, 1135–1136, July 1999.

41. Foran, R., T. Welch, and M. Walker, "Very near ground radio frequency propagation measurements and analysis for military applications," *Proceedings IEEE Military Communications Conference*, Vol. 1, 1356–1360, Atlantic City, NJ, USA, 1999.

42. Feuerstein, M. J., K. L. Blackard, T. S. Rappaport, S. Y. Seidel, and H. H. Xia, "Path loss, delay spread, and outage models as functions of antenna height for microcellular system design," *IEEE Transactions on Vehicular Technology*, Vol. 43, No. 3, 487–498, August 1994.

43. Pascale, A., M. Nicoli, F. Deflorio, B. Dalla Chiara, and U. Spagnolini, "Wireless sensor networks for traffic management and road safety," *IET Intelligent Transport Systems*, Vol. 6, No. 1, 67–77, 2012.

44. Schelkunoff, S. A., "Anatomy of 'surface waves'," *IRE Transactions on Antennas and Propagation*, S133–S139, December 1959.

45. Sommerfeld, A., "Über die ausbreitung der wellen in der drahtlosen telegraphie," *Annalen der Physik*, Vol. 28, No. 4, 665–736, 1909.

46. Norton, K. A., "The physical reality of space and surface waves in the radiation field of radio antennas," *Proceedings of the Institute of Radio Engineers*, Vol. 25, No. 9, 1192–1202, September 1937.

47. Wait, J. R., "A note on surface waves and ground waves," *IEEE Transactions on Antennas and Propagation*, 996–997, November 1965.

48. Schelkunoff, S. A., *Electromagnetic Waves*, D. van Nostrand Company, Inc., Princeton, NJ, 1943.

49. Barlow, H. M. and J. Brown, *Radio Surface Waves*, Oxford University Press, Oxford, 1962.

50. Bremmer, H., "The surface-wave concept in connection with propagation trajectories associated with the sommerfeld problem," *IRE Transactions on Antennas and Propagation*, S175–S182, December 1959.

51. Sarkar, T. K., W. Dyab, M. N. Abdallah, M. Salazar-Palma, M. V. S. N. Prasad, S. Weng Ting, and S. Barbin, "Electromagnetic macro modeling of propagation in mobile wireless communication: Theory and experiment," *IEEE Antennas and Propagation Magazine*, Vol. 54, No. 6, 17–43, December 2012.

52. Sarkar, T. K., W. M. Dyab, M. N. Abdallah, M. Salazar-Palma, M. V. S. N.Prasad, and S.-W. Ting, "Application of the Schelkunoff formulation to the sommerfeld problem of a vertical electric dipole radiating over an imperfect ground," *IEEE Transactions on Antennas and Propagation*, Vol. 62, No. 8, 4162–4170, August 2014.

53. Burrows, C. R., "The surface wave in radio waves over a plane earth," *Proceedings of the IRE*, Vol. 25, 219–229, February 1937.

54. Jeon, T.-I. and D. Grischkowsky, "THz Zenneck surface wave (THz surface plasmon) propagation on a metal sheet," *Applied Physics Letters*, Vol. 88, 2006.

55. Gay-Fernández, J. A., M. G. Sánchez, I. Cuiñas, and A. V. Alejos, "Propagation analysis and deployment of a wireless sensor network in a forest," *Progress In Electromagnetics Research*, Vol. 106, 121–145, 2010.

56. Tokunou, T., R. Yamane, and T. Hamasaki, "Near earth propagation loss model in forest for low power wireless sensor network," *2017 USNC-URSI Radio Science Meeting*, 19–20, 2017.

57. Paul, B. S. and S. Rimer, "A foliage scatter model to determine topology of wireless sensor network," *2012 International Conference on Radar, Communication and Computing (ICRCC)*, 324–328, December 21–22, 2012.

58. Kamarudin, L. M., R. B. Ahmad, B. L. Ong, F. Malek, A. Zakaria, and M. A. Mohd Arif, "Review and modelling of vegetation propagation model for wireless sensor networks using OMNeT++," *IEEE 2010 Second International Conference on Network Applications, Protocols and Services*, 78–83, Kedah, Malaysia, 2010.

59. Oliveira de Medeiros, T. I., Y. P. Molina Rodriguez, F. B. Soares de Carvalho, C. Protásio de Souza, and P. H. Meira de Andrade, "Vegetation encroachment monitoring system for transmission lines using wireless sensor networks," *2018 International Instrumentation and Measurement Technology Conference (I2MTC)*, 1–5, 2018.

60. Comité Consultatif International des Radiocommunications (1986) Inform 236-6: "Influence on terrain irregularities and vegetation on troposphere propagation," *CCIR*, 1986.

61. Weissberger, M. A., "An initial critical summary of models for predicting the attenuation of radio wave by trees," ESD-TR-81-101, Department of Defence, Electromagnetic Compatibility Analysis Center, 1982.

62. Vogel, W. J. and J. Goldhirsh, "Tree attenuation at 869 MHz derived from remotely piloted aircraft measurements," *IEEE Transactions on Antennas and Propagation*, Vol. 34, No. 12, 1460–1464, December 1986.

63. Al-Nuaimi, M. O. and R. B. L. Stephens, "Measurements and prediction model optimisation for signal attenuation in vegetation media at centimetre wave frequencies," *IEE Proceedings on Microwave and Antennas Propagation*, Vol. 145, No. 3, 201–206, June 1998.

64. Meng, Y. S., Y. H. Lee, and B. C. Ng, "Empirical near ground path loss modeling in a forest at VHF and UHF bands," *IEEE Transactions on Antennas and Propagation*, Vol. 57, No. 5, 1461–1468, 2009.

65. Oestges, C., B. Montenegro Villacieros, and D. Vanhoenacker-Janvier, "Radio channel characterization for moderate antenna heights in forest areas," *IEEE Transactions on Vehicular Technology*, Vol. 58, No. 8, 4031–4035, October 2009.

66. Chee, K. L., S. A. Torrico, and T. Kurner, "Radiowave propagation prediction in vegetated residential environments," *IEEE Transactions on Vehicular Technology*, Vol. 62, No. 2, 486–499, February 2013.

67. Sabri, N., S. A. Aljunid, M. S. Salim, R. Kamaruddin, R. B. Ahmad, and M. F. Malek, "Path loss analysis of WSN wave propagation in vegetation," *Journal of Physics: Conference Series 423*, 1–9, 2013.

68. Olasupo, T. O. and C. E. Otero, "The impacts of node orientation on radio propagation models for airborne-deployed sensor networks in large-scale tree vegetation terrains," *IEEE Transactions on Systems, Man, and Cybernetics: Systems*, Vol. PP, No. 99, 1–14, 2017.

Erratum to "Analysis of Propagation for Wireless Sensor Networks in Outdoors"

Giselle M. Galvan-Tejada and Jorge Aguilar-Torrentera

in Progress In Electromagnetics Research B, Vol. 83, 153–175, 2019

Giselle M. Galvan-Tejada[1, 2, *] and Jorge Aguilar-Torrentera[3]

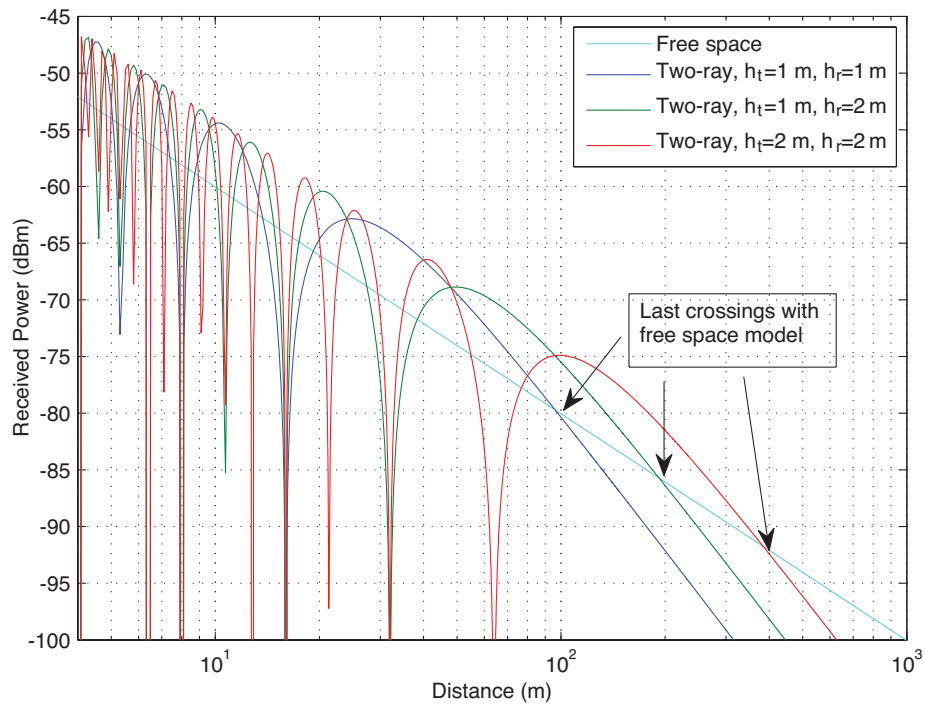All values of axis Y of Figure 8 should be negative as shown below.

Figure 8. Received power for the two-ray model.